



# Performance check of the CsI(Tl) calorimeter for the J-PARC E36 experiment by observing $e^+$ from muon decay

H. Ito<sup>a,\*</sup>, K. Horie<sup>b</sup>, S. Shimizu<sup>b,\*</sup>, S. Bianchin<sup>c</sup>, C. Djalali<sup>d</sup>, B. Dongwi<sup>e</sup>, D. Gill<sup>c</sup>, M.D. Hasinoff<sup>f</sup>, Y. Igarashi<sup>g</sup>, J. Imazato<sup>g</sup>, N. Kalantarians<sup>h</sup>, H. Kawai<sup>i</sup>, S. Kimura<sup>i</sup>, A. Kobayashi<sup>i</sup>, S. Kodama<sup>i</sup>, M. Kohl<sup>e</sup>, H. Lu<sup>d</sup>, O. Mineev<sup>j</sup>, M. Tabata<sup>i</sup>, R. Tanuma<sup>k</sup>, N. Yershov<sup>j</sup>

<sup>a</sup> Department of Physics, Kobe University, Hyogo, 657-8501, Japan

<sup>b</sup> Department of Physics, Osaka University, Osaka, 560-0043, Japan

<sup>c</sup> TRIUMF, Vancouver, V6T 2A3, Canada

<sup>d</sup> Department of Physics and Astronomy, University of Iowa, Iowa City, IA 52242, USA

<sup>e</sup> Physics Department, Hampton University, VA 23668, USA

<sup>f</sup> Department of Physics and Astronomy, University of British Columbia, Vancouver, V6T, 1Z1, Canada

<sup>g</sup> High Energy Accelerator Research Organization (KEK), Tsukuba, 305-0801, Japan

<sup>h</sup> Virginia Union University, Natural Science Department, Richmond, VA 23220, USA

<sup>i</sup> Department of Physics, Chiba University, Chiba, 263-8522, Japan

<sup>j</sup> Institute for Nuclear Research, Moscow, 117312, Russia

<sup>k</sup> Department of Physics, Rikkyo University, Toshima, 171-8501, Japan

## ARTICLE INFO

### Keywords:

Kaon decay

CsI(Tl) calorimeter

Waveform analysis

## ABSTRACT

The J-PARC E36 experiment is searching for lepton universality violation with a stopped kaon beam by measuring the ratio of the  $K^+$  decay widths  $\Gamma(K_{e2})/\Gamma(K_{\mu2}) = \Gamma(K^+ \rightarrow e^+ \nu_e)/\Gamma(K^+ \rightarrow \mu^+ \nu_\mu)$ . Since the radiative  $K^+ \rightarrow e^+ \nu_e \gamma$  decays are backgrounds to be removed in this measurement, the radiated  $\gamma$  rays were detected in a CsI(Tl) calorimeter. The energy calibration for the 768 CsI(Tl) modules was performed using mono-chromatic  $\mu^+$ s from the  $K_{\mu2}$  decays. The delayed  $e^+$  signals from the muon decays were required in order to improve the S/N ratio of the  $K_{\mu2}$  peak by suppressing background events. In addition, a new energy calibration method of the CsI(Tl) calorimeter using stopped cosmic muons has been established.

## 1. Introduction

The  $K^+ \rightarrow l^+ \nu_l$  decay channel is one of the best processes to search for a lepton universality violation [1–3]. The ratio of  $K^+ \rightarrow e^+ \nu_e$  ( $K_{e2}$ ) and  $K^+ \rightarrow \mu^+ \nu_\mu$  ( $K_{\mu2}$ ) decay widths ( $R_K$ ) can be very precisely calculated in the framework of the Standard Model (SM) under the assumption of  $\mu$ – $e$  universality as [4],

$$R_K^{\text{SM}} = \frac{\Gamma(K_{e2})}{\Gamma(K_{\mu2})} = (2.477 \pm 0.001) \times 10^{-5}. \quad (1)$$

In order to compare the experimental  $R_K$  value with the SM prediction, the internal bremsstrahlung process in radiative  $K^+ \rightarrow e^+ \nu_e \gamma$  ( $K_{e2}^{\text{IB}}$ ) and  $K^+ \rightarrow \mu^+ \nu_\mu \gamma$  ( $K_{\mu2}^{\text{IB}}$ ) decay has to be included in the  $K_{e2}$  and  $K_{\mu2}$  samples. On the other hand, the structure dependent processes in radiative  $K^+ \rightarrow e^+ \nu_e \gamma$  ( $K_{e2}^{\text{SD}}$ ) and  $K^+ \rightarrow \mu^+ \nu_\mu \gamma$  ( $K_{\mu2}^{\text{SD}}$ ) decays are

backgrounds and should be removed in the analysis [3]. A deviation of the experimentally measured  $R_K$  from the SM value would lead to a  $\mu$ – $e$  universality violation and indicate the existence of New Physics beyond the SM.

The J-PARC E36 experiment aims to perform a precise  $R_K$  measurement by adopting a stopped  $K^+$  beam method [5,6]. The experiment was performed in 2015. A separated 800 MeV/c  $K^+$  beam was slowed down by a degrader and stopped in a position sensitive  $K^+$  stopper. The momentum measurement of the charged particles was performed using a 12-sector ion-core superconducting toroidal spectrometer, as shown in Fig. 1. The radiated photon from the above radiative processes was measured by a CsI(Tl) calorimeter, an assembly of 768 CsI(Tl) crystals, which covers 75% of the total solid angle. The photon energy and hit position were obtained by summing the energy deposits and by determining the energy-weighted centroid, respectively. Since the SD

\* Corresponding authors.

E-mail addresses: [ito.hiroshi@crystal.kobe-u.ac.jp](mailto:ito.hiroshi@crystal.kobe-u.ac.jp) (H. Ito), [suguru@phys.sci.osaka-u.ac.jp](mailto:suguru@phys.sci.osaka-u.ac.jp) (S. Shimizu).

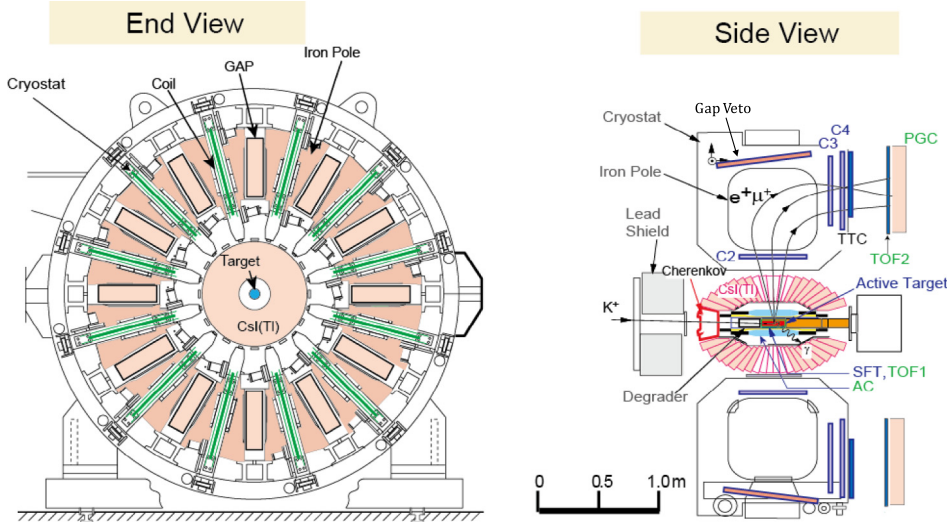


**Fig. 1.** Cross sectional end and side views of the setup for the J-PARC E36 experiment. The momentum vectors of charged particles and photons are determined by the toroidal spectrometer and the CsI(Tl) calorimeter, respectively.

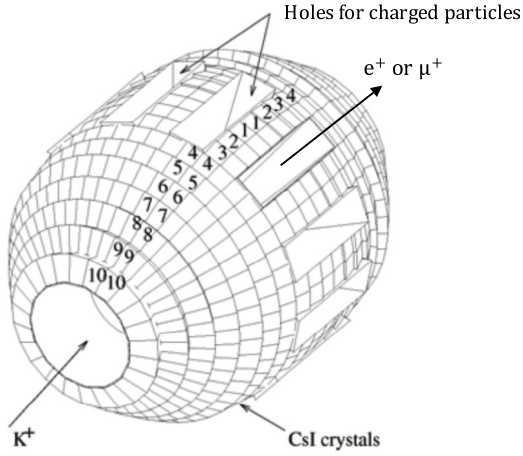


**Fig. 2.** The schematic view of the CsI(Tl) calorimeter. There were 12 holes for outgoing charged particles and 2 holes for the beam entrance and exit. Each crystal had a coverage of  $7.5^\circ$  along both the polar and azimuthal directions.

component subtraction is one of the key issues in E36, the understanding of the CsI(Tl) performance is very important.

This paper is organized as follows. Details of the CsI(Tl) calorimeter and the analysis procedure are described in Sections 2 and 3. In Section 4, a calibration method using the mono-chromatic  $\mu^+$ s from the  $K_{\mu 2}$  decays is explained. A new method of the CsI(Tl) energy calibration using stopped cosmic-ray muons is discussed in Section 5. The results obtained in the present studies are summarized in Section 6.

## 2. CsI(Tl) calorimeter

The CsI(Tl) calorimeter was originally constructed for the KEK-PS E246 experiment to search for a T-violating transverse muon polarization in  $K^+ \rightarrow \pi^0 \mu^+ \nu_\mu$  decay [7–9]. There were 12 holes for outgoing charged particles and 2 holes for the beam entrance and exit, as shown in Fig. 2. Each crystal had a coverage of  $7.5^\circ$  along both the polar and azimuthal directions. The length of the CsI(Tl) crystal was 25 cm which was long enough to neglect shower leakage from the rear end.

Since the CsI(Tl) calorimeter had to be operated under a relatively strong fringing field from the toroidal magnet where PMTs would be

difficult to use, PIN photodiodes (PIN diodes) were employed to read out the scintillation light of the CsI(Tl) crystals. Each crystal with its associated PIN diode and pre-amplifier was assembled in an Al container of 0.1 mm thickness. A charge sensitive pre-amplifier with a time constant of 600  $\mu$ s and a gain of 0.5 V/pC was attached directly to the PIN diode. The output signal from the pre-amplifier was fed to a shaping amplifier with 1  $\mu$ s shaping time. The waveforms of the shaping amplifier outputs were recorded by VF48 flash ADC manufactured by the TRIUMF national laboratory [10]. The VF48 had a 10  $\mu$ s time range and was operated with a 25 MHz external clock signal.

## 3. Waveform analysis

### 3.1. Waveform model

The  $\gamma$ -ray energy and timing can be determined by fitting the CsI(Tl) output signal using a dedicated waveform model function. A typical waveform from the CsI(Tl) calorimeter is shown in the Fig. 3(a), as indicated by black open circles. In the analysis, we adopted the following waveform formula,

$$f(t) = \frac{A}{1 - \exp\{-(t - \tau_0)/\lambda\}} \cdot \text{Freq}\left(\frac{t - \tau_0 - d}{\mu}\right) \cdot \left\{ \frac{t - \tau_0}{\tau_1} \exp\left(1 - \frac{t - \tau_0}{\tau_1}\right) + \varepsilon \frac{t - \tau_0}{\tau_2} \exp\left(1 - \frac{t - \tau_0}{\tau_2}\right) \right\}, \quad (2)$$

where  $A$  is the amplitude of the pulse and  $\tau_0$  is the rise time used for the timing determination. The  $\lambda$ ,  $\mu$  and  $\tau_1$ ,  $\tau_2$  parameters are time constants to express the rise and decay parts of the pulse, respectively.  $d \sim 1$   $\mu$ s is introduced for a timing adjustment and  $\varepsilon \sim 0.06$  is the ratio of the two decay components.  $\text{Freq}(x)$  is known as the frequency function given as

$$\text{Freq}(x) = \frac{1}{\sqrt{2}} \int_{-\infty}^x \exp(-t^2/2) dt. \quad (3)$$

Then, in order to determine these parameters, an equal-weighted  $\chi^2$  quantity is introduced,

$$\chi^2 = \sum_{i=1}^{250} \left\{ A_i - f(t_i) \right\}^2, \quad (4)$$

where  $A_i$  and  $t_i$  are the ADC value and time of the  $i$ th waveform points, respectively.  $A_i$  is an integer number of the VF48 output and the bin by bin errors should be equal among all data points. The parameters in the

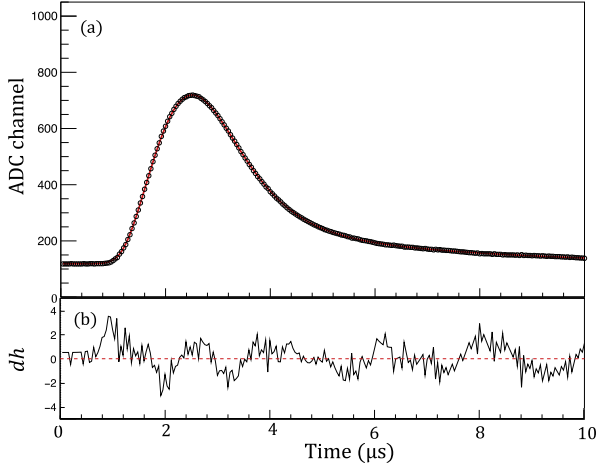


**Fig. 3.** (a) Typical waveform of the CsI(Tl) calorimeter signal. The open circles are the data and the red line is a fitting result of the waveform model. (b) The deviation of the data points from the fitting result. (For interpretation of the references to colour in this figure legend, the reader is referred to the web version of this article.)

model function were derived by minimizing the  $\chi^2$  values. The red line in Fig. 3(a) is the fitting result using the above method, and the deviation of each data point ( $dh$ ) is shown in Fig. 3(b). Typical  $\chi^2$  values are distributed in the region of 100–500 (the number of degrees of freedom =  $250 - 8 = 242$ ) which is mainly due to the imperfect reproducibility of the CsI(Tl) output by the waveform model.

### 3.2. Pulse separation of pileup events

For the analysis of pileup events, the maximum  $dh$  value ( $dh_{\max}$ ) was first determined in the entire region using a single-pulse fitting. The waveforms with  $|dh_{\max}| > 10$  can be recognized as two or more pulse components. The deviation of the data points from the single-pulse fitting result for a typical pileup event is shown in Fig. 4(b), black line. These events were treated as pileup events, and multiple pulses in the fitting were taken into account. Then, the  $\chi^2$  value using a double-pulse waveform was again minimized by changing the fitting parameters. A typical pileup waveform is shown in Fig. 4(a), black open circles. We can accept events as a double-pulse waveform with the conditions of (i) a waveform with  $|dh_{\max}| < 10$  and (ii) the time interval between the 1st and the 2nd signals is greater than 200 ns. The rejected events are treated as events with further multiple signals. The red and green solid lines in Fig. 4(a) are the fitting results using the single-pulse and double-pulse fitting functions, respectively. The associated decomposed pulses are shown as the green (1st pulse) and blue (2nd pulse) dotted lines. The thick red line in Fig. 4(b) shows the  $dh$  distribution assuming the double-pulse fittings, which indicates successful pulse separation using the double-pulse fitting.

## 4. CsI(Tl) calibration using $K_{\mu 2}$ decay events

### 4.1. Background reduction by observing the $e^+$ from $\mu^+$ decay

The CsI(Tl) energy calibration was performed using mono-chromatic  $\mu^+$ s from the  $K_{\mu 2}$  decays at rest in the  $K^+$  stopping target. The original  $\mu^+$  kinetic energy from stopped kaon decays was 152.5 MeV. These muons were stopped in the CsI(Tl) crystal after losing their energies in the target and generated the delayed  $e^+$  signal from the subsequent  $\mu^+ \rightarrow e^+ \bar{\nu}_\mu \nu_e$  decay. The  $e^+$  signal can be observed as the second pulse in the waveform analysis using the double-pulse fitting.

The  $K_{\mu 2}$  events were selected by the following conditions: (I) the number of hit crystals was only one, (II) the first pulse time coincided

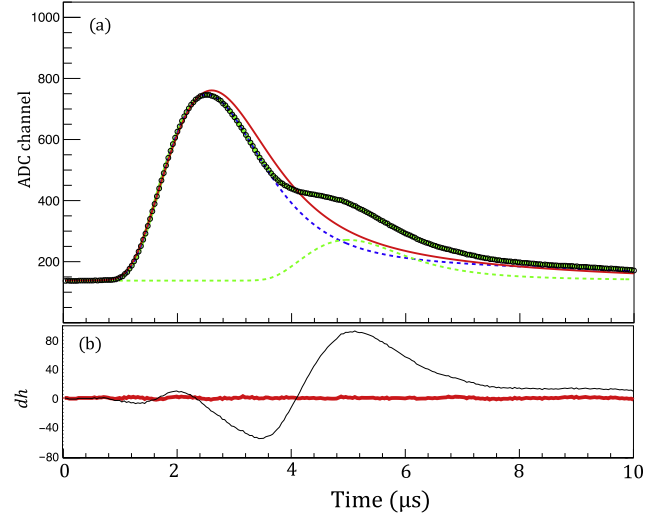


**Fig. 4.** (a) Typical pileup waveform of the CsI(Tl) calorimeter signal. The open circles are the data points. The red and green lines are the results adopting the single- and double-pulse fitting function. The green and blue dotted lines are the decomposed 1st and 2nd pulses. (b) The deviation of each data point from the fit curves. The black and red lines are the results using the single and double fitting, respectively. (For interpretation of the references to colour in this figure legend, the reader is referred to the web version of this article.)

with the  $K^+$  decay, and (III) the waveform data was successfully analyzed as a double-pulse waveform.

The pulse height spectrum obtained by selecting events with only the conditions (I) and (II) are shown in Fig. 5 as the black histogram. On the other hand, the red filled histogram represents events selected with all the above conditions. It is clearly seen that background components below the  $K_{\mu 2}$  peak are significantly suppressed by requiring the  $\mu^+$  decay in the CsI(Tl). Here, the backgrounds are considered to be mainly accidental events created by the beam particles.

Then, the signal to noise ratio ( $S/N$ ) was calculated as,

$$S/N = \frac{N(500 \leq l < 800)}{N(l < 500, 800 \leq l)}, \quad (5)$$

where  $l$  is the pulse height of the first pulse obtained by the fitting. The  $K_{\mu 2}$  peak region and the background dominant region were separated as  $N(500 \leq l < 800)$  and  $N(l < 500, 800 \leq l)$ , respectively. The  $S/N$  ratio was determined to be  $\sim 0.4$  for the events selected with the conditions of (I) and (II). Next, the  $\mu^+$  selection by requiring the double-pulse waveform was performed, and the  $S/N$  was obtained to be  $\sim 4$ . Thus, we can conclude that the requirement of the  $\mu^+$  stop and decay in the CsI(Tl) is a very useful technique to reduce the backgrounds from the beam particles and make the CsI(Tl) energy calibration significantly more accurate.

### 4.2. CsI(Tl) performance check

For the CsI(Tl) energy calibration, the  $\mu^+$  energy loss in the target system should be added to the  $\mu^+$  energy observed by the CsI(Tl). The energy conversion factor,  $k$ , can be formulated as  $k = (152.5 - E_t \text{ MeV})/l$ , where  $E_t$  is the muon energy loss in the target. The  $\mu^+$  path length in the target was obtained by connecting the CsI(Tl) center of the  $\mu^+$  hit module and the  $K^+$  vertex position determined by the target system. The typical  $k$  value was obtained to be  $2.1\text{--}2.5 \text{ MeV}^{-1}$ . Then, the  $\mu^+$  energy spectrum from the  $K_{\mu 2}$  decay is obtained by taking into account the energy loss in the target as  $E = kl + E_t$ , as shown in Fig. 6. The red and blue spectra indicate the calibrated energy spectrum with and without the target energy correction, respectively. The target energy correction improved the energy resolution to  $\sigma = 2.63\%$  from  $4.73\%$ .

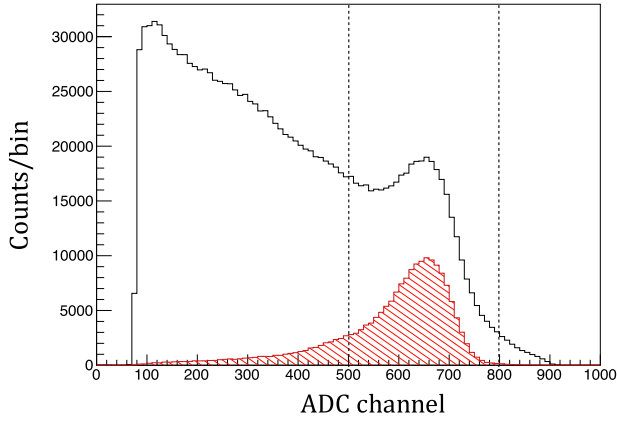


**Fig. 5.** Integrated pulse-height spectrum. The black spectrum shows the events selected with the conditions of (I) and (II). The red shaded histogram shows the events selected with all the conditions. The region indicated by the two dotted lines is used to estimate the S/N ratio.

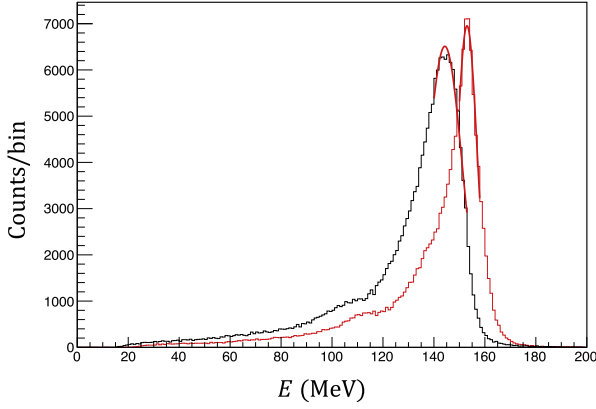


**Fig. 6.** The calibrated energy spectra obtained using the  $K^+ \rightarrow \mu^+ \nu_\mu$  decays. The red spectrum includes a correction for the energy loss in the target. The red lines are the fitting results assuming a Gaussian function. (For interpretation of the references to colour in this figure legend, the reader is referred to the web version of this article.)

Also, the CsI(Tl) timing information was checked by requiring the  $e^+$  signals to reduce the effects from accidental backgrounds. The 40 ns clock timing uncertainty of VF48 was corrected for by measuring the trigger signal timing using the same VF48 module ( $T_{\text{ref}}$ ). Fig. 7 shows the  $\mu^+$  timing distribution obtained from the  $\tau_0$  parameter corrected for  $T_{\text{ref}}$ ,  $\tau_0 - T_{\text{ref}}$ . The timing resolution was determined to be  $\sigma = 10.7 \pm 0.1$  ns by fitting the distribution with a Gaussian function, as shown by the red line in Fig. 7.

##### 5. A new method of energy calibration using stopped cosmic-ray muons

It is possible to consider a new CsI(Tl) calibration method using stopped cosmic-ray muons with the subsequent  $e^+$  emission in the CsI(Tl) calorimeter [11]. This method is proposed to measure the  $e^+$  energy spectrum for a rough CsI(Tl) energy calibration without using the  $K_{\mu 2}$  decays. Since the maximum  $e^+$  energy from the muon decay is 52.32 MeV, the energy calibration can be performed by measuring the  $e^+$  energy after the cosmic-ray muon stops in the CsI(Tl) crystal. The cosmic muons stop homogeneously in the CsI(Tl), and we do not need to consider the specific structure of the CsI(Tl) calorimeter.

The energy distribution of the decomposed second pulse is shown in Fig. 8 as indicated by the black dots. Here the calibration parameters

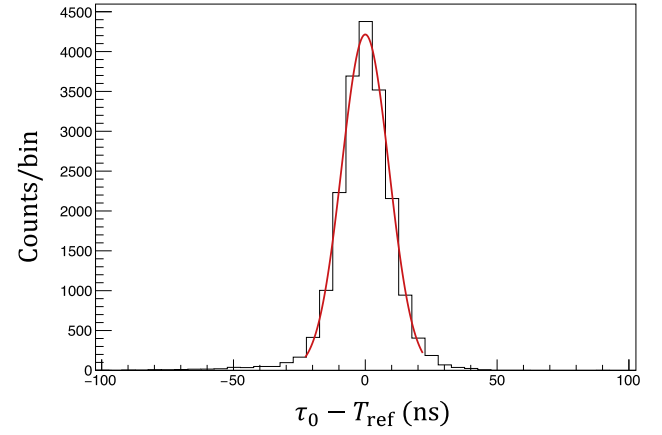


**Fig. 7.** The  $\mu^+$  timing distribution corrected for  $T_{\text{ref}}$  ( $\tau_0 - T_{\text{ref}}$ ). The timing resolution was determined to be  $\sigma = 10.7 \pm 0.1$  ns. (For interpretation of the references to colour in this figure legend, the reader is referred to the web version of this article.)

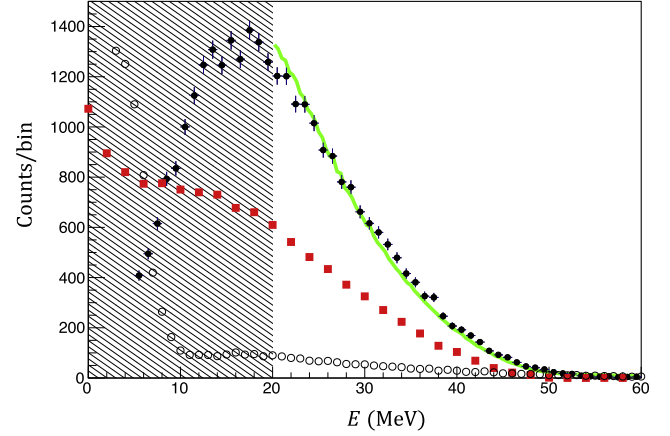


**Fig. 8.** Energy distributions of  $e^+$  ( $e^-$ ) from stopped cosmic muons. The red squares and black open circles are the calculated  $e^+$  and  $e^-$  energy distributions, respectively. An electromagnetic gamma shower was taken into account in the simulation. The black hatched area is not used in the fitting because of the online threshold setting of 20 MeV.

obtained from the  $K_{\mu 2}$  decays were used. The red squares and black open circles are the calculated  $e^+$  and  $e^-$  energy distributions from stopped cosmic  $\mu^+$  and  $\mu^-$  decays, respectively, obtained using a Monte Carlo simulation based on a GEANT4 code. Electromagnetic shower leakage from the muon stopped module was taken into account. The energy distributions were calculated by varying the muon yield ratio of  $F_+/F_- = 1.1$ – $1.6$  [12–16] and compared with the experimental one. The green line shown in Fig. 8 is the result with  $F_+/F_- = 1.6$ . The energy resolution of 2.63% in  $\sigma$  obtained from the  $K_{\mu 2}$  calibration result has been used.

In order to determinate the energy calibration parameters using stopped cosmic-ray muons, a common gain parameter relative to the energy coefficients obtained from the  $K_{\mu 2}$  calibration results was introduced. The reduced  $\chi^2_{\text{v}}/\text{NDF}$  determined by comparing the experimental data with the simulation was calculated as a function of the above relative gain coefficient, as shown in Fig. 9, where NDF is the number of degrees of freedom. The black dots and open squares correspond to the results obtained by assuming  $F_+/F_- = 1.1$  and  $1.6$ , respectively. It should be noted that the fitting region was chosen to be 20–60 MeV because the online energy threshold was set to 20 MeV. Scattering of the  $\chi^2_{\text{v}}$  values is due to random smearing to account for the CsI(Tl) energy

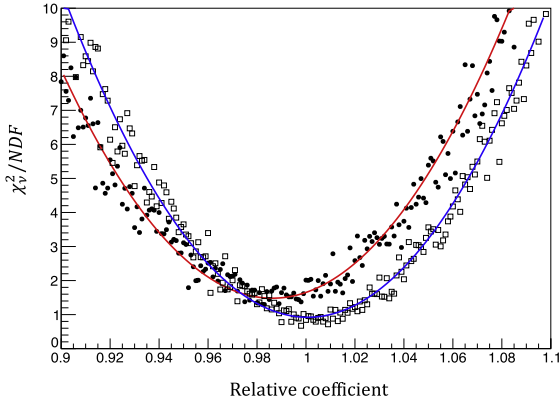


**Fig. 9.** Reduced  $\chi^2$  obtained by changing the relative gain coefficient. The black dots and open squares correspond to the results obtained by assuming  $F_+/F_- = 1.1$  and  $1.6$ , respectively. The lines in the figure represent the fitting results using a parabolic function. The gain coefficients obtained from the stopped cosmic muons are consistent with those from the  $K_{\mu 2}$  events within 3%–4%.

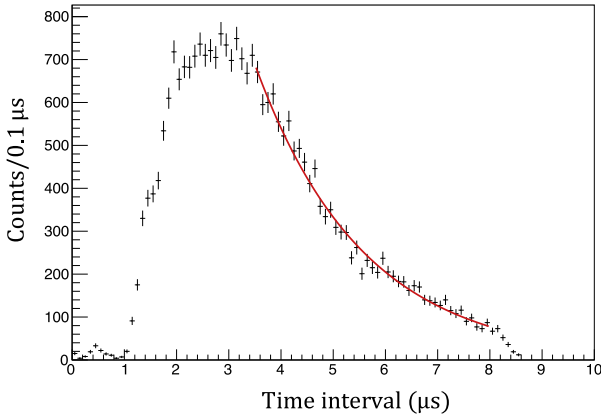


**Fig. 10.** Time interval between cosmic muons and the delayed  $e^+$  ( $e^-$ ) signals through the  $\mu \rightarrow e\nu\bar{\nu}$  decays. The black dots and the red line are the data and fitting function, respectively.

resolution. The lines in the figure represent the fitting results using a parabolic function. As a result, the relative coefficients for  $F_+/F_- = 1.1$  and  $1.6$  were determined to be  $0.986 \pm 0.033$  and  $1.001 \pm 0.032$ , which indicates the gain coefficients obtained from the stopped cosmic muons are consistent with those from the  $K_{\mu 2}$  events at the 3%–4% level. Therefore, the experimental data were in good agreement with the above two simulation models, indicating a correct understanding of the  $e^+$  and  $e^-$  behavior generated from the stopped muons.

The muon lifetime curve was also measured using the time interval between the 1st and 2nd pulses, as shown in Fig. 10 by the black dots.

The pulse separation efficiency of events with the first and second pulse time difference shorter than  $1 \mu\text{s}$  is very low. The fall off of the data points higher than  $8 \mu\text{s}$  is due to the finite  $10 \mu\text{s}$  window of the VF48. Fitting the data with an exponential function, the decay constant was determined to be  $2.06 \pm 0.03 \mu\text{s}$  ( $\chi^2/NDF = 69.5/43$ ), as shown by the red line. The fitting region of  $3.5$ – $8.0 \mu\text{s}$  was chosen, since the second pulse separation efficiency was not significantly high out of this region. The observed time constant is a little shorter than the PDG value which indicates that most of the  $\mu^-$  events are captured by CsI nuclei and do not contribute to the above lifetime measurement.

## 6. Conclusion

A model function for the waveform analysis of the CsI(Tl) calorimeter in the E36 experiment has been developed, and the information of the decomposed second pulses can be used for the event selection. The CsI(Tl) energy calibration was successfully performed by choosing the  $K_{\mu 2}$  events, and imposing the existence of the second pulses, and the S/N ratio was significantly improved. Then, the CsI(Tl) performance was carefully checked by studying the energy and timing resolutions.

A new energy calibration method using stopped cosmic muons is proposed. The energy and timing of the delayed  $e^+$  ( $e^-$ ) signals were determined by the decomposed second pulse in the double-pulse waveform analysis. The observed energy spectrum is consistent with the simulation calculation with an accuracy of 3%–4%, indicating the establishment of a new calibration method without using any accelerator facilities.

## Acknowledgments

This work was supported by a Grant-in-Aid for Scientific Research (C), No. 15K05113, from the Japan Society for the Promotion of Science (JSPS) in Japan and by NSERC (SAPPJ-2017-00034) and NRC (TRIUMF) in Canada. The authors thank H. Yamazaki for encouragement in executing this work. We would like to thank the J-PARC staff for the excellent beam delivery during our experimental beamtime.

## References

- [1] G. Lamanna, et al., Nucl. Part. Phys. Proc. 273–275 (2016) 1671.
- [2] C. Lazzeroni, et al., Phys. Lett. B 719 (2013) 326.
- [3] F. Ambrosino, et al., Europ. Phys. J. C 64 (2009) 627.
- [4] V. Cirigliano, I. Rosell, Phys. Rev. Lett. 99 (2007) 231801.
- [5] S. Shimizu, et al., Proposal for J-PARC 50 GeV Proton Synchrotron, 2010, P36 Jun.
- [6] S. Strauch, et al., Proc. Sci., PoS(KAON13)014, 2013.
- [7] M. Abe, et al., Phys. Rev. D 73 (2006) 072005.
- [8] J.A. Macdonald, et al., Nucl. Instrum. Methods A 506 (2003) 60.
- [9] D.V. Dementyev, et al., Nucl. Instrum. Methods A 440 (2000) 151.
- [10] Y. Igarashi, M. Saito, IEEE 2012 Nuclear Science Symposium and Medical Imaging Conference Record (NSS/MIC), <http://dx.doi.org/10.1109/NSSMIC.2012.6551335>.
- [11] H. Ito, et al., IEEE 2016 Nuclear Science Symposium and Medical Imaging Conference Record (NSS/MIC), <http://dx.doi.org/10.1109/NSSMIC.2016.8069751>.
- [12] S. Haino, et al., Phys. Lett. B 594 (2004) 35.
- [13] P. Archard, et al., Phys. Lett. B 598 (2004) 15.
- [14] P. Adamson, et al., Phys. Rev. D 76 (2007) 052003.
- [15] V. Khachatryan, et al., Phys. Lett. B 692 (2010) 83.
- [16] N. Agafonova, et al., Eur. Phys. J. C 67 (2010) 25.